Geochemical Journal, Vol. 49, pp. 139 to 155, 2015 doi:10.2343/geochemj.2.0337

Fluid inclusions study and direct $^{40}Ar/^{39}Ar$ dating by *in vacuo* crushing of quartz veins within UHP metamorphic rocks from Yuka terrane, North Qaidam orogen, China

RONGGUO HU,[1,2,3]* JAN R. WIJBRANS,[2] FRAUKJE M. BROUWER,[2] LINGHAO ZHAO,[1]
MIN WANG[1,3] and HUANING QIU[1]

[1]State Key Laboratory of Isotope Geochemistry, Guangzhou Institute of Geochemistry, Chinese Academy of Sciences, Guangzhou 510640, P.R. China
[2]Department of Earth Sciences, VU University Amsterdam, De Boelelaan 1085, 1081 HV Amsterdam, The Netherlands
[3]University of Chinese Academy of Sciences (UCAS), Beijing 100049, P.R. China

(*Received July 21, 2013; Accepted September 22, 2014*)

Characterization and *in vacuo* crushing $^{40}Ar/^{39}Ar$ dating have been performed on four quartz veins within ultrahigh pressure (UHP) metamorphic rocks from the Yuka terrane, North Qaidam Orogen, western China. The data are used to decipher the nature, origin and age of the vein-forming fluids during the exhumation of UHP rocks. By using petrography and microthermometry analyses, three principal types of fluid inclusions have been identified: (1) hypersaline inclusions (type-a), (2) intermediate to high-salinity inclusions (type-b), and (3) low-salinity aqueous inclusions (type-c). The type-a and partly type-b inclusions occur as isolated, suggesting a primary origin. Most of the type-b inclusions occur as cluster in crystal micro-fracture, but never crosscut the crystal boundaries between individual quartz grains, indicating they are pseudo-secondary inclusions. The type-c inclusions commonly distributed in trails along the micro-fracture, suggesting a secondary origin. Quartz samples dated by $^{40}Ar/^{39}Ar$ *in vacuo* crushing method yield monotonic declining release patterns: anomalously old apparent ages are obtained at the first steps and relative flat age plateaus (429–411 Ma) over the final several steps. The gases liberated in the final steps are most derived from radiogenic and trapped argon in small primary fluid inclusions and pseudo-secondary fluid inclusions and also atmospheric argon from the crusher. Consequently, the plateau ages are concluded as the best estimate for the ages of quartz veining during the UHP rocks exhumation. Meanwhile, we ascribe the extremely high initial apparent ages to the most easily crushed and excess ^{40}Ar ($^{40}Ar_E$) dominated secondary fluid inclusions, because they generally distributed along crystal fractures. On the plots of $^{40}Ar^*/^{39}Ar_K$ vs. $^{38}Ar_{Cl}/^{39}Ar_K$, the early data points yield well-defined isochrons and with two group ages: 392 Ma and ~344 Ma, representing two episodes of post-collisional fluid flow activities. Microthermometry analyses and $^{40}Ar/^{39}Ar$ *in vacuo* crushing dating suggest that the secondary inclusions may be originated from the excess ^{40}Ar rich post-hydrothermal fluid from the depth. In contrast, the primary inclusions have more complex origins, including meteoric waters transported by fault/shearing zones, retrograde decomposition of hydrous minerals and partial melt of HP/UHP rocks.

Keywords: North Qaidam orogen, quartz vein, fluid inclusions, $^{40}Ar/^{39}Ar$ dating, *in vacuo* crushing

INTRODUCTION

There are abundant quartz-veins within eclogite-facies HP/UHP metamorphic rocks of continental collision zones, which were formed due to water–rock interaction resulted by localized fluid (Selverstone *et al*., 1992; Yardley and Bottrell, 1992; Rubatto *et al*., 1999; Zheng *et al*., 2003, 2007; Wu *et al*., 2009) or large-scale transport (Nelson, 1991; John *et al*., 2008). Based upon field occurrences, mineral assemblages and formation stages, three groups of HP/UHP quartz vein can generally be distinguished: synmetamorphic veins, early retrograde veins and late retrograde veins (Becker *et al*., 1999; Rubatto *et al*., 1999; Franz *et al*., 2001; Li *et al*., 2001a; Rubatto and Hermann, 2003; Wu *et al*., 2009; Sheng *et al*., 2012).

As a significant indicator of fluid flow and thus, a potential source of important vital information for fluid processes in subduction/exhumation zones, quartz veins within UHP rocks have attracted extensive scientific interest. however, most previous geochemical studies have concentrated on fluid inclusion composition, hydrogen/oxygen stable isotopes and quartz micro-structure studies (Becker *et al*., 1999; Franz *et al*., 2001; Li *et al*., 2001b; Xiao *et al*., 2002; Zheng *et al*., 2003, 2011; Nuhter and Stokhert, 2007; Birtel and Stokhert, 2008; Zhang *et al*., 2008). In the previous geochronological studies, only a

*Corresponding author (e-mail: hurongguo@163.com)

Copyright © 2015 by The Geochemical Society of Japan.

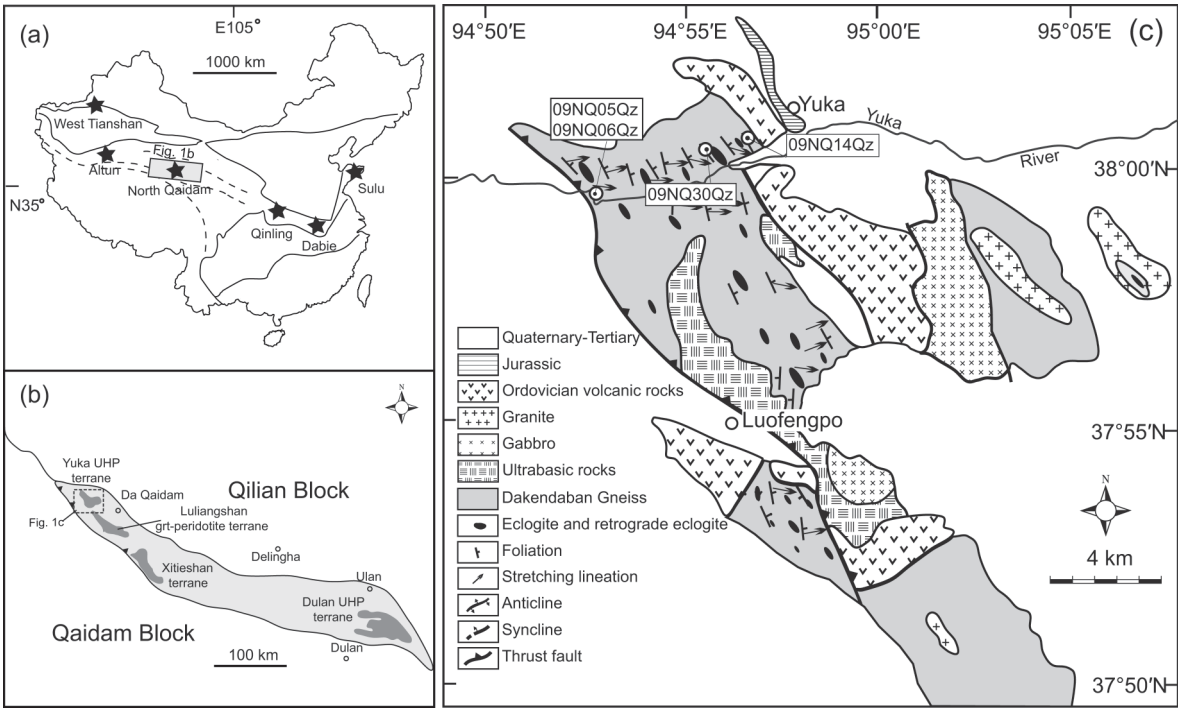

Fig. 1. (a) Geological sketch map showing the locality of north Qaidam orogen in China; (b) distribution of UHP metamorphic terranes in the North Qaidam orogenic belt; (c) sketch map of the Yuka terrane and sample localities. (modified after Zhang et al., 2005)

few Rb–Sr isochron studies of fluid-inclusions within quartz from the eclogites have been reported (Wang *et al*., 2000, 2003). Currently, most studies focus on the selection of accessory minerals like zircon and rutile for U–Pb dating, or coexisting minerals such as muscovite for $^{40}Ar/^{39}Ar$ dating (Franz *et al*., 2001; Gao *et al*., 2006; Zheng *et al*., 2007; Wu *et al*., 2009; Zong *et al*., 2010; Chen *et al*., 2012; Sheng *et al*., 2012), to constrain the time of quartz vein formation. Unfortunately in the case of $^{40}Ar/^{39}Ar$ dating of micas, the occurrence of excess ^{40}Ar within HP/UHP muscovite in many cases may obscure the geological information contained within these mica crystals (Li *et al*., 1994). Meanwhile, accessory minerals in quartz veins are often too scarce and too small to be used for isotopic dating, and when present, they may have formed after crystallization of the quartz vein. Consequently, the results of isotopic dating studies may not always precisely represent the formation ages of the veins.

The formation age of quartz veins may alternatively be constrained directly by applying $^{40}Ar/^{39}Ar$ dating by *in vacuo* crushing, as the dating is based on the age information obtained from K and Ar dissolved in the fluid inclusions (Kelley *et al*., 1986; Turner, 1988; Qiu *et al*., 2002; Kendrick *et al*., 2006). Quartz is a good mineral for such an approach as it is nominally free of K, and is relatively free from impurities in the crystal and commonly has a high abundance of fluid inclusions. Also, the slow rate of lattice diffusion of argon in quartz indicates that quartz may have a relatively high closure temperature for argon diffusion (Clay *et al*., 2010). An additional benefit of $^{40}Ar/^{39}Ar$ dating is the neutron induced production of $^{39}Ar_K$, $^{38}Ar_{Cl}$ and $^{37}Ar_{Ca}$, which are formed during neutron irradiation for $^{40}Ar/^{39}Ar$ dating and can be used as proxies for the K, Cl and Ca concentration in the fluid. As such they can be used to obtain additional information on the chemistry of the postulated reservoirs (Kelley *et al*., 1986; Turner and Bannon, 1992).

Fluid inclusions are commonly encapsulated by quartz crystals during first growth and in later stages by crack-seal mechanisms (Roedder, 1984). The primary fluid inclusions (PFIs) composition reflects the composition of the fluids trapped during diagenesis or the early stages of metamorphism, and is commonly an aqueous fluid with variable levels of salinity. Secondary fluid inclusions (SFIs) are introduced when cracks develop that are subsequently sealed by precipitation of minerals.

Over the past 10 years, considerable progress has been made in the study of the petrology, mineralogy, geochemistry and geochronology of HP/UHP metamorphic rocks and granites of the Yuka terrane, north Qaidam orogen, Qinghai Province, western China (Chen *et al*., 2005, 2009; Zhang *et al*., 2005; Yin *et al*., 2007; Menold

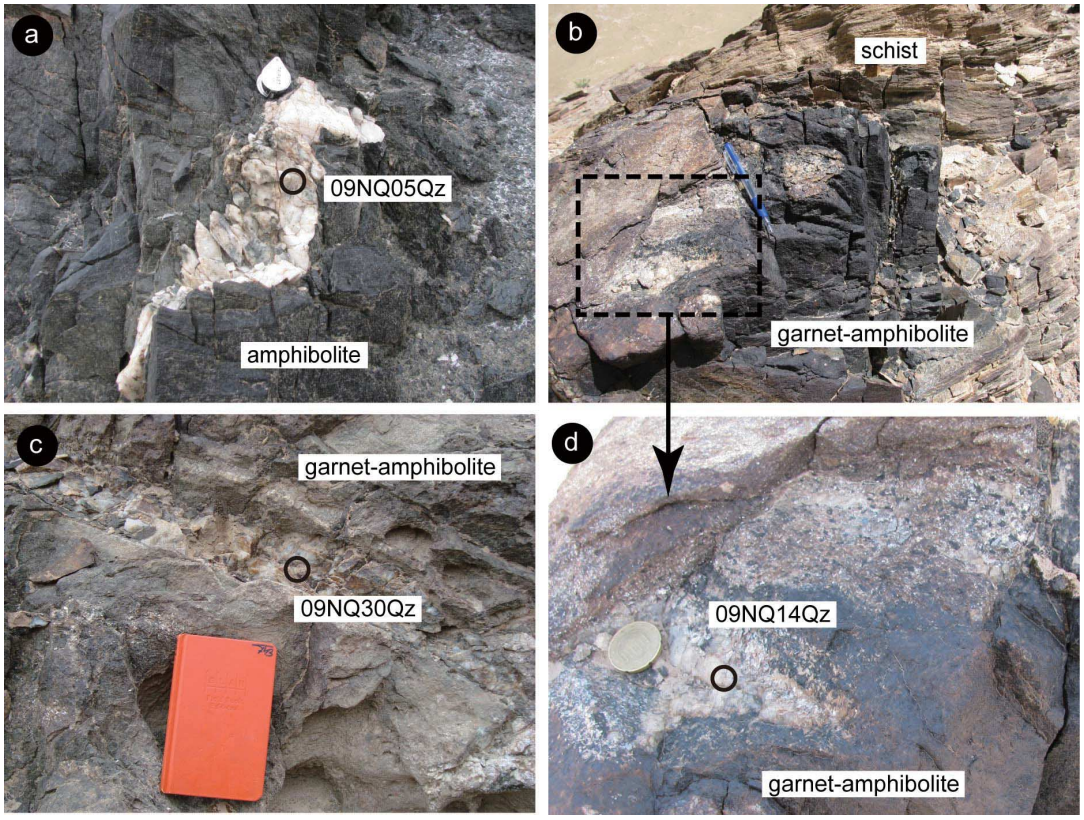

Fig. 2. Field photographs of quartz veins and host garnet-amphibolites in the Yuka terrane, North Qaidam orogen. Open circles denote the sample locality for quartz veins. The diameter of the hand lens and coin used in (a) and (d) is 2.5 cm; the length of the pen and notebook in (b) and (c) is 14 and 16 cm respectively.

et al., 2009; Zhang *et al*., 2009; Wang *et al*., 2013). As yet, there are no studies that have focused on fluid inclusions, separately, or in combination with direct isotopic dating of the quartz veins. Here we present a study using, a combined approach of petrographic observation, microthermometric measurement and $^{40}Ar/^{39}Ar$ *in vacuo* and crushing dating, that is the first of its kind of the Yuka HP-terrane quartz veins. The objective of our study is to decipher the origin of fluid flow and to further constrain the timing of quartz vein formation using a direct approach.

Geological Setting and Samples

The north Qaidam orogen is a long and narrow HP/UHP metamorphic belt which located between the Qilian block and Qaidam block (Figs. 1a and b). It is starting from Shaliuhe–Yematan in Dulan, Qinghai province, and then extending north-westward through Xitieshan, Luliangshan, to Yuka for about 400 km (Yang *et al*., 2001, 2005). Three eclogite-gneiss units and one garnet–peridotite–gneiss unit base on different rock paragenesis have been recognized in this UHP metamorphic belt (Zhang *et al*., 2005; Mattinson *et al*., 2007). From east to north, they are: (1) the Dulan eclogite–gneiss unit; (2) the Xitieshan eclogite–gneiss unit; (3) the Luliangshan garnet peridotite–gneiss unit; and (4) the Yuka eclogite–gneiss unit (Fig. 1b). Coesite have been recognized as inclusions in zircon from the north Dulan paragneiss and Xitieshan garnet–amphibolite, as well as in garnet from the Yuka eclogite (Yang *et al*., 2001; Zhang *et al*., 2009; Liu *et al*., 2012). In contrast, inclusion of micro-diamond in zircon and sodic–amphibole exsolutions in garnet were only reported and confirmed in the Luliangshan garnet–peridotite (Song *et al*., 2005).

The present research area Yuka unit is the westernmost terrane in the North Qaidam orogen (Figs. 1b and c). In this UHP terrane, eclogite and associate retrograde production occur as lenses, pods or layers within gneiss and schist. Fresh eclogite chiefly consists of garnet + omphacite + phengite + rutile + quartz, corresponding to peak metamorphic conditions of $T = 566–680°C$, $P = 2.9–3.4$ GPa (Chen *et al*., 2005; Zhang *et al*., 2009). The existing geochronological data shows that there are two groups with regard to peak eclogite-facies metamorphism: 495–488 Ma by zircon TIMS U–Pb method (Zhang *et al*.,

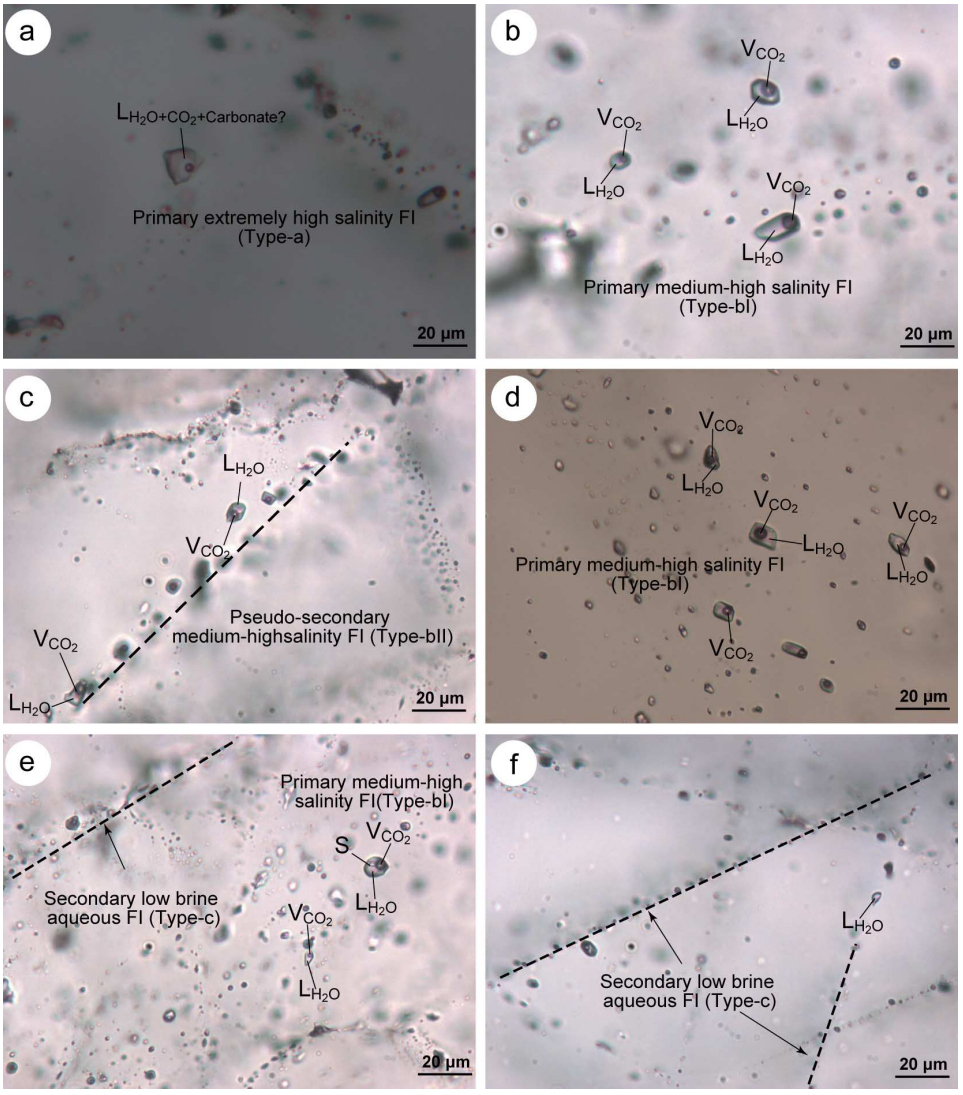

Fig. 3. Photomicrographs of fluid inclusions in quartz from Yuka. (a) a isolated hypersaline salinity inclusions (type-a, primary, 09NQ14Qz); (b) isolated medium-high salinity inclusions (type-bI, primary, 09NQ14Qz); (c) along micro fractures but terminating at grain boundaries medium-high salinity fluid inclusions (type-bII, pseudo-secondary, 09NQ14Qz); (d) isolated and clustered medium-high salinity inclusions (type-bI, primary, 09NQ05Qz); (e) isolated medium-high salinity inclusions with solid-phase (S) occasionally (type-bI, primary, 09NQ06Qz), and low brine aqueous fluid inclusions (type-c, secondary, 09NQ06Qz) trapped along a healed fracture; (f) along healed fractures and cross-cutting grain boundary low brine aqueous fluid inclusions (type-c, secondary, 09NQ30Qz). Broken lines in c, e and f denote healed/micro fractures.

2005) and 436–431 Ma by zircon LA-ICPMS U–Pb method (Chen *et al*., 2009). It is suggested that the TIMS U–Pb results of 495–488 Ma are probably mixed ages of metamorphic domains and residual cores (Chen *et al*., 2007, 2009).

Eclogites are commonly overprinted by amphibolite-facies retrogression with variably size quartz veins/lenses in Yuka terrane. The quartz veins filling in the fractures of host rocks occur as thin tubes, or occurring as thin sheets on the surface of the metabasites (Fig. 2). Quartz sample 09NQ05Qz formed in a fracture of a garnet–amphibolite block and is *ca*. 50 cm in length and 2–5 cm in width. It contents is 95 wt.% of quartz, with minor paragenetic minerals including amphibole, feldspar and chlorite (Fig. 2a). Sample 09NQ06Qz was taken from an outcrop in the vicinity of 09NQ05Qz, and is characterized by a similar field occurrence, mineral assemblage and textural features. Sample 09NQ14Qz occurs as thin layer on the surface of a tectonically elongated retrograde eclogite block (Fig. 2b). It has a size of *ca*. 6 × 8 cm, a medium to fine grained texture, and a smoky gray colour. Its quartz content is *ca*. 85% and coexisting with miner-

Table 1. Characteristics and microthermometeric data of fluid inclusions in Yuka quartz veins

Sample number	Type of inclusions*	Distributions of inclusions	Final melting temperature (°C)	Homogenization temperature (°C)	Salinity wt.% NaCl eq.	No.
09NQ14Qz	Type-a	Isolated	–39 to –30.5	242–200	35.2–29	6
	Type-b	Isolated, clustered or along fractures	–24 to –10.5	237–208	25–14.5	7
	Type-c	Along fractures	–6 to –2.1	245–227	9.2–3.5	8
09NQ05Qz	Type-b	Isolated or along fractures	–24 to –13	250–174	25–16.9	15
	Type-c	Along fractures	–7 to –3.1	238–154	10.5–5.1	15
09NQ06Qz	Type-b	Along fractures	–23 to –15	223–187	24.3–18.6	10
	Type-c	Along fractures	–1.2 to –1.1	225–190	2.1–1.9	4
09NQ30Qz	Type-b	Isolated or along fractures	–14.5 to –7.3	240–180	18.5–10.9	13
	Type-c	Along fractures	–5.9 to –3.9	230–186	9.1–6.3	13

**Type-a = Hypersaline primary inclusions; Type-b = Intermediate to high-salinity primary and pseudo-secondary fluid inclusions; Type-c = Low-salinity secondary aqueous inclusions; No.: total numbers of measured fluid inclusions.*

als include white mica and amphibole (Fig. 2d). Sample 09NQ30Qz is from a 150 cm long and 10 cm wide milky quartz vein, with a quartz content of *ca*. 95%. It is cutting through a phengite-bearing garnet–amphibolite lens and quartz in the vein is coexisting with amphibole, chlorite and feldspar (Fig. 2c).

Analytical Methods

Fluid inclusions heating and freezing measurements were performed on doubly polished thick sections of four high pressure quartz vein samples using a Linkam MDS 600 freezing/heating stage coupled to a BX51 Olympus polarizing microscope, with nitrogen as the cooling medium, at State Key Laboratory of Geological Processes and Mineral Resources, China University of Geosciences, Wuhan, China. The lower and upper temperature limits of the Linkam MDS 600 instrument are –195°C and +600°C, respectively. For temperatures below +30°C precision and accuracy are ±0.2°C, for temperatures between +30 and +300°C, ±1°C, higher about ±2°C. The heating/freezing stage was calibrated with pure CO_2 in natural fluid inclusions. The rate of heating and cooling are normally ~10°C/min and reduced to 2°C/min near phase changes. Phase transitions in aqueous inclusions are best defined by the terminology proposed by Roedder (1984). The homogenization temperatures (T_h) of aqueous fluid inclusions that homogenize to the liquid phase and the temperatures of ice-melting (T_m) were measured. Homogenization temperatures are the minimum trapping temperatures, whereas ice-melting temperatures provide a measure of the fluid salinity (Hall *et al*., 1988).

Hand samples were crushed and sieved to obtain a size fraction (250–500 μm). Quartz grains were separated using standard separation methods followed by handpicking under a binocular microscope to confirm that the sample is pure quartz grain. Samples were then wrapped in Al foil and located into quartz tubes together with standards and irradiated at the TRIGA reactor at the Oregon State University Reactor Centre. Irradiation duration was 20 h for irradiation VU83. Correction factors for interferences of Ca and K isotopes are: $(^{39}Ar/^{37}Ar)_{Ca} = 0.000673$, $(^{36}Ar/^{37}Ar)_{Ca} = 0.000264$, $(^{40}Ar/^{39}Ar)_{K} = 0.00086$ and $(^{38}Ar/^{39}Ar)_{K} = 0.01211$. As a flux monitor standards for *j-value* calculation for this project, DRA1 sanidine with an assumed age of 25.26 Ma was used (Wijbrans *et al*., 1995).

In vacuo crushing experiments were carried out in an in-house designed crushing apparatus which was connected to a three stage extraction line and a quadrupole mass spectrometer in the argon isotope laboratory in VU University Amsterdam (Schneider *et al*., 2009). The detailed experimental process is as same as the description by Qiu and Wijbrans (2006). Samples were loaded into a 40 cm long, 4 cm diameter Inconel® tube and crushed by an iron pestle that is lifted and dropped with a frequency of one time per second (1 Hz) using external electromagnet-control. Before analyses, the crushers were baked overnight at 250°C. The extracted gases were first passed through the cryotrap to adsorb the moisture from the fluid inclusions, and then purified at 250°C by a Fe/V/Zr getter pump and 450°C by a Zr/Al getter pump. The purification process lasted for around 16 minutes before the gases were analysed for the determination of the argon isotopic ratios in the mass spectrometer. Experiments began and ended with cold blank analyses to correct for system blanks with the procedure described above but without moving the pestle.

Table 2. Complete $^{40}Ar/^{39}Ar$ crushing in vacuo data

Step	Pestle drop numbers	$^{36}Ar_{air}$	$^{37}Ar_{Ca}$	$^{38}Ar_{Cl}$	$^{39}Ar_{K}$	$^{40}Ar^{*}$	Age ± 2σ (Ma)	$^{40}Ar^{*}$ (%)	$^{39}Ar_{K}$ (%)
1) Quartz 09NQ05Qz by *in vacuo* crushing, J = 0.00478855, I_0 = 295.5, Yuka terrane									
1	4	2068.479	688.717	343.533	379.086	1094530.255	4864.5 ± 24.2	64.17	2.11
2	6	957.964	391.442	217.870	243.508	685478.621	4821.9 ± 30.7	70.77	1.35
3	12	1079.031	649.940	276.766	332.158	922013.127	4798.3 ± 24.1	74.30	1.85
4	20	560.248	637.481	164.977	204.300	538735.221	4712.4 ± 25.3	76.49	1.14
5	40	517.555	1007.227	152.922	227.432	490813.766	4380.0 ± 22.4	76.24	1.26
6	60	920.162	1558.284	129.279	279.392	416624.598	3782.9 ± 11.4	60.51	1.55
7	60	376.865	1663.140	84.928	268.481	283394.615	3248.8 ± 29.6	71.79	1.49
8	80	401.226	2550.383	73.829	329.431	251735.612	2776.2 ± 24.2	67.98	1.83
9	150	602.299	4661.390	77.996	563.622	318504.122	2363.3 ± 15.9	64.15	3.13
10	300	926.935	9574.903	55.642	750.961	179910.474	1378.6 ± 18.1	39.64	4.17
11	300	867.072	13506.576	60.359	1135.359	221868.133	1191.6 ± 11.8	46.41	6.31
12	300	561.403	14369.854	33.277	1226.589	168283.081	911.0 ± 9.9	50.36	6.82
13	300	639.634	16800.402	33.109	1351.355	134259.949	702.1 ± 9.3	41.53	7.51
14	300	370.563	17144.420	18.761	1270.684	102347.219	588.5 ± 5.3	48.31	7.06
15	300	359.676	17466.635	0.000	1150.389	78052.640	507.6 ± 8.0	42.34	6.39
16*	350	450.593	18277.362	12.711	1244.126	67430.595	416.3 ± 10.7	33.62	6.91
17*	400	425.368	18886.883	11.828	1076.960	59241.987	421.8 ± 10.5	32.03	5.98
18*	500	427.522	20508.299	16.905	1116.849	61464.745	422.0 ± 11.9	32.73	6.21
19*	650	461.374	22294.559	2.026	1098.507	58919.289	412.4 ± 14.9	30.18	6.10
20*	700	490.304	18370.669	18.213	881.160	48322.840	420.7 ± 11.9	25.01	4.90
21*	900	645.710	18344.740	28.993	862.381	46900.855	417.6 ± 19.7	19.73	4.79
22*	1200	793.722	16810.293	17.937	828.541	45307.843	419.6 ± 19.5	16.19	4.60
23*	1300	686.670	12229.890	9.847	659.777	35704.098	415.7 ± 17.4	14.96	3.67
24*	1200	921.119	8087.859	4.735	516.106	27167.031	405.5 ± 32.1	9.08	2.87
2) Quartz 09NQ06Qz by *in vacuo* crushing, J = 0.00474416, I_0 = 295.5, Yuka terrane									
1	4	514.068	35.012	98.978	73.123	497981.980	6324.8 ± 42.4	76.63	2.63
2	8	404.465	49.576	93.876	80.236	483094.184	6109.6 ± 30.6	80.17	2.89
3	12	134.635	26.963	27.739	33.075	170858.783	5843.3 ± 98.6	81.11	1.19
4	30	302.755	91.884	70.896	70.077	348466.099	5777.3 ± 32.4	79.57	2.52
5	60	228.627	133.234	34.119	60.900	230781.665	5309.9 ± 69.6	77.35	2.19
6	120	346.863	175.912	37.401	84.247	204377.027	4557.9 ± 46.2	66.60	3.03
7	300	644.929	428.486	39.828	165.420	207742.528	3499.7 ± 35.2	52.15	5.95
8	300	406.758	402.710	21.240	139.532	121724.295	2952.9 ± 36.6	50.32	5.02
9	400	521.662	416.398	17.399	163.513	110355.391	2589.8 ± 38.7	41.72	5.88
10	500	612.393	407.946	19.038	158.772	72697.187	2082.7 ± 35.3	28.66	5.71
11	500	606.242	393.017	7.960	134.202	39186.537	1568.3 ± 52.8	17.95	4.83
12	700	800.983	527.465	12.716	166.663	29940.760	1112.1 ± 78.0	11.23	5.99
13	800	717.200	629.612	8.535	179.570	21447.495	809.9 ± 63.5	9.19	6.46
14	900	552.553	676.004	0.000	174.519	16580.105	671.2 ± 60.8	9.22	6.28
15	1000	755.539	499.813	4.009	162.330	12578.414	564.8 ± 70.2	5.33	5.84
16*	1000	585.137	455.951	2.997	192.981	10559.183	416.3 ± 61.0	5.76	6.94
17*	1100	1032.041	341.304	14.218	161.336	8516.070	403.2 ± 98.1	2.72	5.80
18*	1200	1014.384	287.136	15.924	153.021	8415.939	418.3 ± 100.5	2.73	5.50
19*	1400	1111.804	250.705	19.463	161.053	8401.345	398.9 ± 106.2	2.49	5.79
20*	1100	1453.466	249.851	18.161	126.866	6697.216	403.2 ± 172.2	1.54	4.56
21*	1100	1591.420	237.607	13.274	139.491	7383.401	404.2 ± 170.6	1.55	5.02

Table 2. (continued)

Step	Pestle drop numbers	$^{36}Ar_{air}$	$^{37}Ar_{Ca}$	$^{38}Ar_{Cl}$	$^{39}Ar_{K}$	$^{40}Ar^{*}$	Age ± 2σ (Ma)	$^{40}Ar^{*}$ (%)	$^{39}Ar_{K}$ (%)
3) Quartz 09NQ14Qz by *in vacuo* crushing, J = 0.00463596, I_0 = 295.5, Yuka terrane									
1	4	581.496	167.643	68.578	73.854	3814121.224	9890.6 ± 31.2	95.69	1.35
2	8	366.231	157.661	49.129	71.894	3195171.167	9620.9 ± 39.8	96.72	1.31
3	8	273.856	116.660	30.951	39.295	1710704.125	9583.9 ± 40.2	95.48	0.72
4	12	135.044	142.580	18.936	35.112	1239984.889	9208.4 ± 73.6	96.88	0.64
5	20	145.588	188.280	18.044	41.943	1248707.302	8902.4 ± 56.0	96.67	0.77
6	30	153.257	190.768	16.273	42.419	876738.511	8249.7 ± 58.3	95.09	0.78
7	60	261.593	327.798	15.635	87.357	990052.728	7181 ± 35.4	92.76	1.60
8	100	206.893	600.340	21.759	137.035	1056394.272	6501.6 ± 17.1	94.53	2.50
9	150	288.341	754.040	16.868	207.371	709683.423	5097 ± 15.7	89.28	3.79
10	200	251.830	935.460	14.678	271.176	580355.620	4313.1 ± 18.5	88.63	4.96
11	200	292.556	662.071	7.043	201.299	282880.698	3638.6 ± 22.2	76.59	3.68
12	240	277.375	833.998	5.419	215.637	300996.116	3628.1 ± 17.8	78.60	3.94
13	300	285.960	964.231	13.393	283.678	256327.302	2970.5 ± 25.3	75.21	5.19
14	300	208.421	788.310	1.390	216.514	141758.105	2516.8 ± 12.9	69.71	3.96
15	300	238.675	766.658	7.366	189.759	95566.065	2172.8 ± 20.7	57.54	3.47
16	300	177.704	730.936	2.786	183.468	66723.739	1782.5 ± 17.3	55.96	3.35
17	360	260.729	780.886	2.805	197.898	56110.501	1513.9 ± 14.2	42.14	3.62
18	400	229.690	932.446	6.516	196.966	38251.120	1158.2 ± 11.6	36.04	3.60
19	400	184.681	903.455	0.000	184.143	28295.803	970.4 ± 13.4	34.15	3.37
20	450	238.507	961.902	2.443	204.246	27002.620	862.4 ± 13.5	27.70	3.73
21	550	268.350	1086.155	0.000	268.502	27265.568	696 ± 13.8	25.59	4.91
22	550	298.689	1066.291	0.259	201.239	15485.682	550.4 ± 15.8	14.93	3.68
23*	600	232.571	1018.483	1.101	195.149	11597.821	439 ± 17.1	14.44	3.57
24*	700	296.281	1724.753	3.098	363.036	21424.427	436.3 ± 14.1	19.66	6.64
25*	900	387.347	1387.151	3.459	173.153	10168.760	434.4 ± 21.0	8.16	3.17
26*	1000	554.215	1373.983	2.402	269.602	15278.755	420.8 ± 16.8	8.53	4.93
27*	1100	957.088	1265.613	2.744	315.728	18605.124	435.7 ± 24.7	6.17	5.77
28*	1000	738.836	1129.308	9.887	335.727	19005.310	420.4 ± 20.3	8.01	6.14
29*	900	444.801	1137.485	6.701	267.623	15178.819	421.1 ± 14.2	10.35	4.89
4) Quartz 09NQ30Qz by *in vacuo* crushing, J = 0.00581866, I_0 = 295.5, Yuka terrane									
1	10	396.297	195.274	27.507	29.755	1235143.466	9906.5 ± 114.4	91.34	1.04
2	20	213.664	349.000	15.602	26.561	808905.506	9350.4 ± 116.7	92.76	0.92
3	30	226.057	387.767	16.683	35.931	784179.118	8753.3 ± 96.8	92.15	1.25
4	50	208.894	582.294	12.033	47.486	585317.861	7733.4 ± 95.5	90.46	1.65
5	80	201.419	681.017	13.712	64.004	458396.246	6771.7 ± 82.7	88.51	2.23
6	120	217.254	1254.164	4.954	108.527	401560.972	5619.4 ± 35.7	86.22	3.78
7	200	308.880	2084.268	10.081	153.158	332873.055	4714.9 ± 40.8	78.48	5.33
8	300	315.733	3028.377	9.980	178.718	299197.945	4283 ± 29.9	76.23	6.22
9	400	465.978	3341.153	11.663	172.578	263593.886	4133.6 ± 38.1	65.69	6.01
10	450	532.047	3335.455	5.015	160.465	174201.966	3590.4 ± 42.5	52.56	5.59
11	500	516.804	3471.231	8.512	154.134	100571.165	2828.6 ± 43.3	39.71	5.37
12	550	504.242	3531.370	0.000	152.861	68128.491	2307.5 ± 42.5	31.38	5.32
13	600	412.615	4007.924	8.322	148.882	48022.861	1906.4 ± 52.7	28.26	5.18
14	700	556.960	4252.299	2.774	218.599	30857.093	1081.7 ± 57.6	15.79	7.61
15	800	208.559	2177.060	1.231	155.763	8729.740	509.2 ± 31.0	12.41	5.42
16*	850	149.405	1901.499	1.139	221.462	9954.344	419.1 ± 28.4	18.40	7.71
17*	900	205.229	1499.328	0.000	149.819	6913.945	429.1 ± 31.2	10.23	5.22
18*	900	116.201	1777.858	0.596	131.603	5895.278	417.9 ± 41.2	14.65	4.58

These $^{40}Ar/^{39}Ar$ experiments were measured using a Quadrupole mass spectrometer in VU University Amsterdam. The argon isotopes are listed in cps.

**Steps were included in the calculation for the isochron ages.*

$^{40}Ar^{*}$: air- and K ($^{40}Ar_K$) corrected ^{40}Ar, $^{40}Ar^{*} = {}^{40}Ar_m - 295.5 \times {}^{36}Ar_{air} - 0.00086 \times {}^{39}Ar_K$, where "m" means measure data.

RESULTS

Fluid inclusion analyses

First, petrographic observation and microthermometric measurements have been applied to the vein quartz samples from the Yuka terrane. The total salinities (W) are calculated with the reduction formula based on the final ice-melting temperatures ($|T_m|$) (Hall *et al.*, 1988): $W = 1.78|T_m| - 0.0442|T_m|^2 + 0.000557|T_m|^3$. Two or three single fluid inclusions in each cluster were selected for measurement. In total, about 88 fluid inclusions in quartz were investigated. Final melting and homogenization temperatures were measured on the same inclusions where possible.

Based on the textural criteria (primary fluid inclusions (PFIs) occur as isolated, randomly and clustered distributed inclusions; pseudo-secondary fluid inclusions were identified as those that formed in healed fractures terminating at grain boundaries and growth zones; secondary fluid inclusions (SFIs) were identified in healed fractures cross-cutting grain boundaries and growth zones) that was proposed by Roedder (1984), three principal types of fluid inclusions have been distinguished. Examples of textural setting and typical occurrences of fluid inclusions are shown in Fig. 3. The different textural types also correspond with different fluid compositions and densities. As shown in Table 1, hypersaline, intermediate to high-salinity and low-salinity aqueous fluid inclusions are grouped as type-a, type-b and type-c, respectively.

Hypersaline inclusions (type-a) are extremely rare and were only observed in sample 09NQ14Qz. The size of these inclusions is in the range of 10–15 μm; they display isolated distributions and regular morphologies, suggesting a primary origin. These inclusions may represent the oldest recognizable generation of fluid inclusions found in this study. Most of these inclusions are two-phase (liquid-vapor) inclusions with an extremely small CO_2 bubble at room temperature (Fig. 3a). These inclusions usually froze at around –80 to –160°C, and showed a granular texture between –55 and –42°C on subsequent heating, that was interpreted as a transition from metastable non-crystalline to a crystalline state. The brines have final ice melting temperatures (T_m) between –39 and –30.5°C, corresponding to extremely high salinities of 35.2–29 wt.% NaCl equivalent. Homogenization temperatures (homogenization to the liquid phase; T_h) are between 242 to 200°C.

Intermediate to high-salinity fluid inclusions (type-b) have been observed in all the quartz samples. They are the predominant type and very abundant in all measured samples. Based on textural criteria, the type-b inclusions are subdivided into type-bI and type-bII types. The type-bI inclusions are 5–20 μm in size, displaying negative crystal morphologies and observed as isolated, random or clustered distributions, suggesting a primary origin (Figs. 3b, d and e). They are commonly two-phase inclusions (liquid-vapor, CO_2 + H_2O) at room temperature, occasionally containing solid-phases (Fig. 3e). In contrast, the type-bII inclusions mostly occur in microfractures that never crosscut the crystal boundaries between individual quartz grains (Fig. 3c), indicating they are pseudo-secondary rather than secondary inclusions (Roedder, 1984). Heating-freezing stage analysis shows that the type-b inclusions have T_m between –24 and –7.3°C, corresponding to salinities of 25–10.9 wt.% NaCl equivalent. The homogenization temperature is between 250 and 174°C.

Low-salinity aqueous inclusions (type-c) have also been distinguished in all quartz samples, and occur along cross-cutting healed fractures, indicating their secondary origin (Figs. 3e and f). They are 0.5–20 μm in size, commonly showing compositions with two-phase (CO_2 + H_2O), but pure aqueous inclusions have been observed occasionally. The measured results gave T_m values between –7 and –1.1°C, corresponding to salinities of 10.5–1.9 wt.% NaCl equivalent. Values for T_h were measured between 245 and 154°C.

$^{40}Ar/^{39}Ar$ plateau and isochron ages

The $^{40}Ar/^{39}Ar$ data were calculated and plotted using the ArArCALC software package of Koppers (2002). $^{40}Ar/^{39}Ar$ analytical data are listed in Table 2. Age spectra and inverse isochrons for each of the samples are illustrated in Figs. 4 to 8. Both the plateau and inverse isochron age uncertainties are given at the 2σ level.

The apparent age spectrum for sample 09NQ05Qz consists of 24 steps, with in total more than 9000 times pestle drops during progressive crushing. This quartz sample exhibits a monotonically declining release spectrum: the first segment yielded anomalously old apparent ages that decrease from the initial crushing steps and the final steps form a flat plateau with concordant apparent ages. Apparent ages decrease from 4865 to 508 Ma with steps 1 to 15. On the inverse isochron diagram of $^{36}Ar/^{40}Ar$ vs. $^{39}Ar/^{40}Ar$, the data points gradually move from near the origin of the diagram to the atmospheric argon component end member along with the Y axis ($^{36}Ar/^{40}Ar$) (Fig. 4b). A reliable plateau age with 418.5 ± 4.7 Ma (MSWD = 0.3, $^{39}Ar_K$ = 46%) is obtained from steps 16–24. The data points constituting the plateau form a well-defined isochron with an intercept age of 421.7 ± 5.1 Ma (MSWD = 0.3) on the inverse isochron diagram, corresponding to an initial $^{40}Ar/^{36}Ar$ ratio of 295 ± 1 (Fig. 4b).

In vacuo crushing $^{40}Ar/^{39}Ar$ analyses of the other three quartz samples yielded similarly shaped age spectra. All spectra with abnormally old apparent ages during the first several steps, then a significant decrease during following steps and finally the occurrence of flat plateaux with

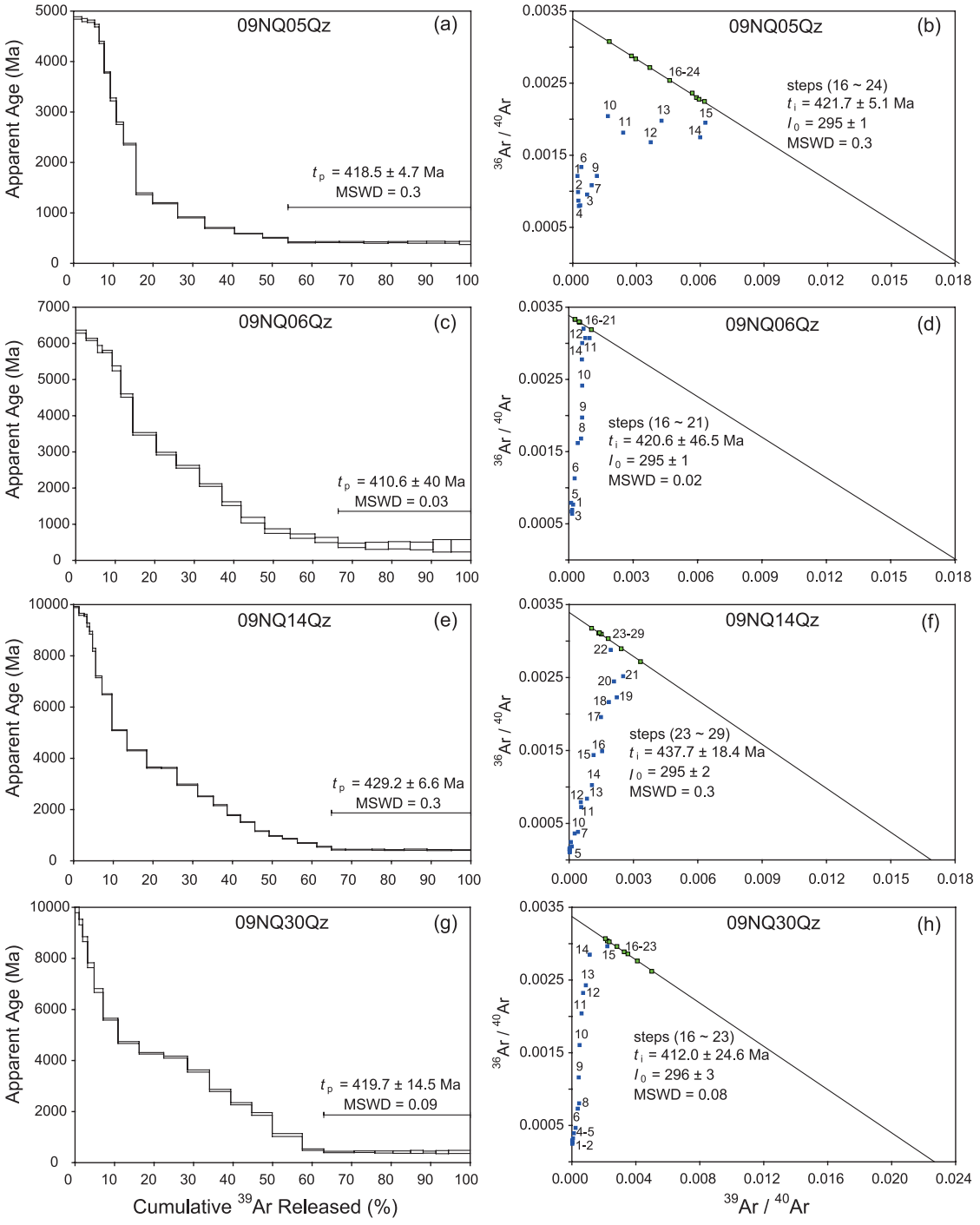

Fig. 4. Apparent age spectra (left) and inverse isochrons ($^{36}Ar/^{40}Ar$ vs. $^{39}Ar/^{40}Ar$) (right) of quartz from the Yuka terrane by in vacuo crushing. Apparent ages are obtained by excluding non-radiogenic ^{40}Ar with modern atmospheric $^{40}Ar/^{36}Ar$ ratios of 295.5.

Silurian–Devonian plateau ages of 410.6 ± 40 Ma (MSWD = 0.03, $^{39}Ar_K$ = 34%), 429.2 ± 6.6 Ma (MSWD = 0.3, $^{39}Ar_K$ = 35%) and 419.7 ± 14.5 Ma (MSWD = 0.09, $^{39}Ar_K$ = 37%), for samples 09NQ06Qz, 09NQ14Qz and 09NQ30Qz, respectively (Figs. 4c, e and g). The data points of the plateaux form well-defined isochrons on inverse isochron plots of $^{36}Ar/^{40}Ar$ vs. $^{39}Ar/^{40}Ar$, with ages of 420.6 ± 46.5 Ma, 437.7 ± 18.4 Ma and 412 ± 24.6 Ma,

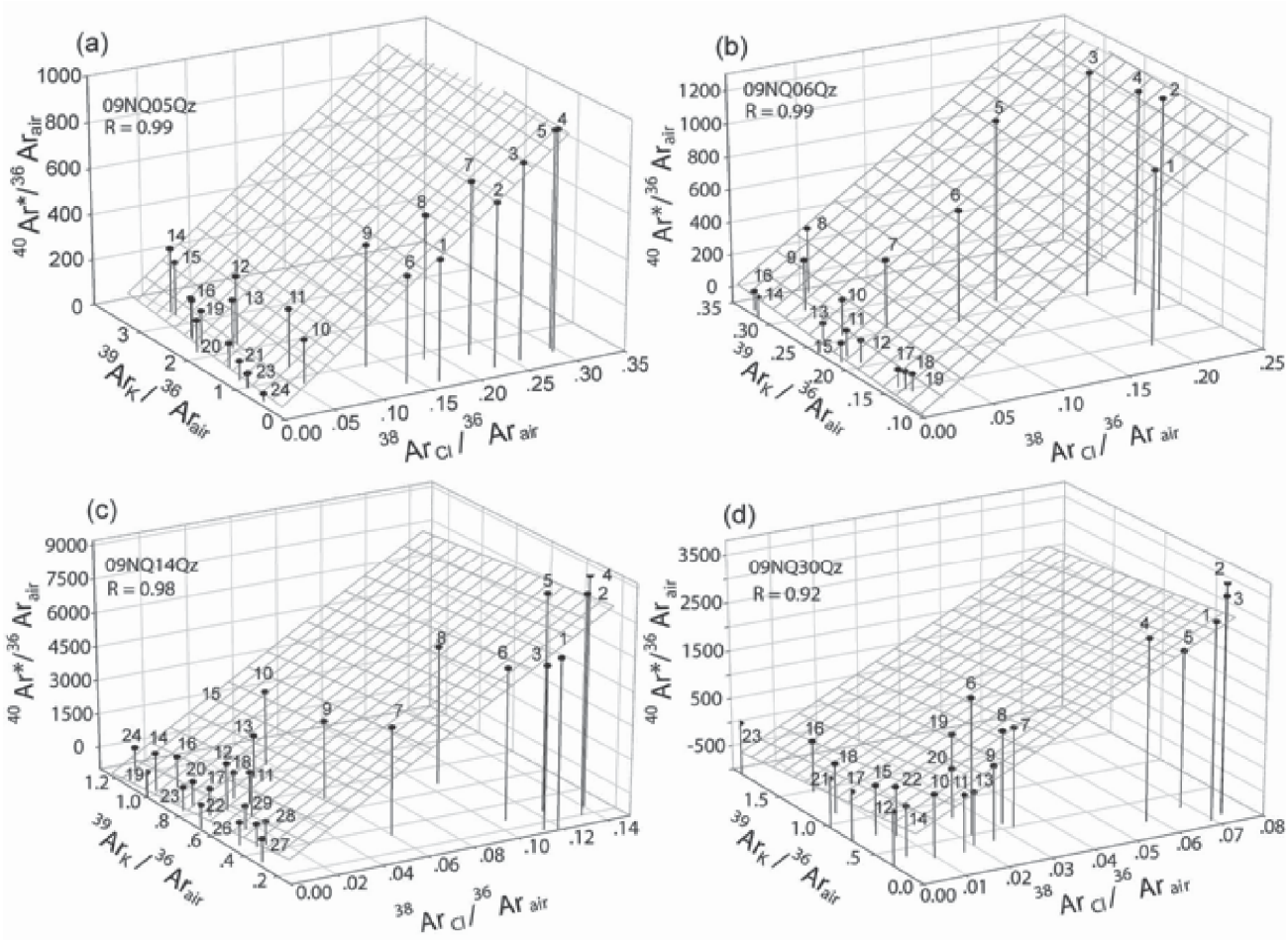

Fig. 5. $^{40}Ar^*$–^{36}Ar-$^{39}Ar_K$–$^{38}Ar_{Cl}$ *3D correlation diagrams for Yuka quartz veins. Here, "R" represents correlations between* $^{40}Ar^*$ *and* $^{38}Ar_{Cl}$.

respectively (Figs. 4d, f and h). The initial $^{40}Ar/^{36}Ar$ ratios of all isochrons are indistinguishable from the modern atmospheric ratio of 295.5.

Correlations between Cl and K derived Ar isotopes

To search for elemental correlations, we performed multiple regressions on the amount of $^{40}Ar^*$, K-derived $^{39}Ar_K$, Cl-derived $^{38}Ar_{Cl}$ and air-derived ^{36}Ar with the aim of identifying the different Ar sources in the fluid inclusions (Kelley *et al*., 1986; Turner, 1988; Turner and Bannon, 1992; Kendrick *et al*., 2001; Qiu and Wijbrans, 2006, 2008; Jiang *et al*., 2012; Bai *et al*., 2013). Here, $^{40}Ar^*$ denotes total ^{40}Ar just minus atmospheric ^{40}Ar ($^{40}Ar_A$) and ^{40}Ar ($^{40}Ar_K$) produced by neutron irradiation, including both K *in situ* decay derived radiogenic ^{40}Ar ($^{40}Ar_R$) and parentless excess ^{40}Ar ($^{40}Ar_E$). The neutron-induced argon isotopes of $^{38}Ar_{Cl}$ and $^{39}Ar_K$ are used to represent Cl and K contents, respectively.

Three axes diagrams for $^{40}Ar^*/^{36}Ar$ vs. $^{39}Ar_K/^{36}Ar$ vs. $^{38}Ar_{Cl}/^{36}Ar$ based on isotopic analyses of Yuka quartz samples by crushing are shown in Fig. 5. In the plot, two ^{40}Ar end-member components: air ($^{40}Ar_A$ and ^{36}Ar) and fluid can be seen. The fluid is rich in $^{40}Ar_E$ and Cl, and probably rich in K if K-bearing daughter minerals exist. On the $^{40}Ar^*$–$^{39}Ar_K$–$^{38}Ar_{Cl}$ plane as shown in Fig. 5, the crushing data points of the first several steps have relatively high $^{38}Ar_{Cl}/^{36}Ar$ and $^{40}Ar^*/^{36}Ar$ combined with low $^{39}Ar_K/^{36}Ar$ ratios. Moreover, the data shows that there is a good correlation between the $^{40}Ar^*$ and $^{38}Ar_{Cl}$ which define a plane with high correlation coefficients of 0.92–0.99 (Fig. 5). Detailed correlations and the significance of these K and Cl derived Ar isotopes will be shown and discussed in the following sections.

$^{40}Ar^*/^{38}Ar_{Cl}$ vs. $^{39}Ar_K/^{38}Ar_{Cl}$

The plots of $^{40}Ar^*/^{38}Ar_{Cl}$ vs. $^{39}Ar_K/^{38}Ar_{Cl}$ based on isotopic analyses of Yuka quartz samples by *in vacuo* crushing are collected in Fig. 6. Similar to the features of many crushing experiments on UHP metamorphic garnet (Qiu and Wijbrans, 2006, 2008), the data points of the

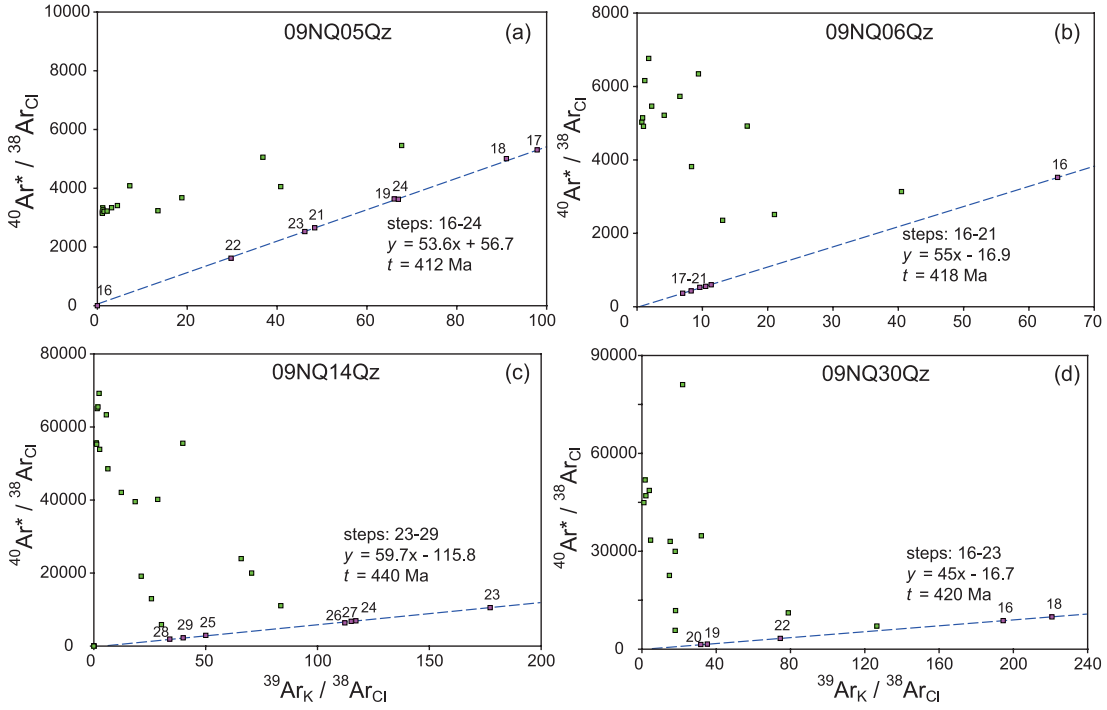

Fig. 6. Plots of $^{40}Ar^*/^{38}Ar_{Cl}$ vs. $^{39}Ar_K/^{38}Ar_{Cl}$ based on the $^{40}Ar/^{39}Ar$ data of the quartz samples by crushing in vacuo. These data points (pink points and with crushing steps number) defining the age plateaux also define correlation lines with slopes corresponding to ages of 412, 418, 440 and 420 Ma for 09NQ05Qz, 09NQ06Qz, 09NQ14Qz and 09NQ30Qz, respectively.

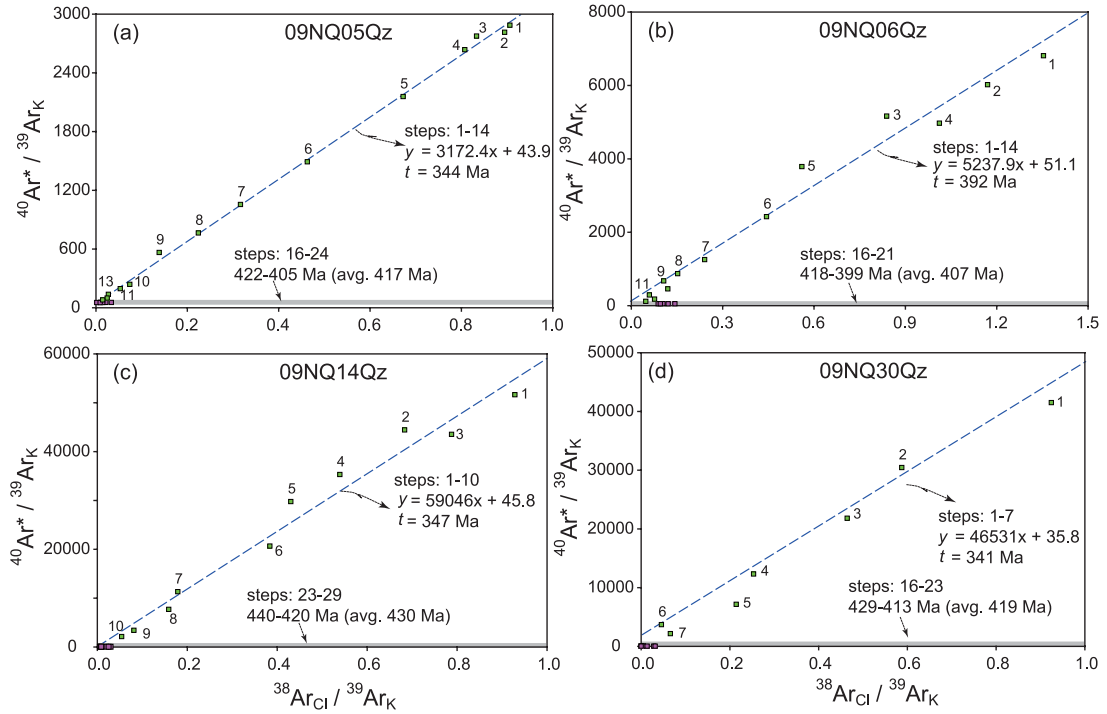

Fig. 7. Plots of $^{40}Ar^*/^{39}Ar_K$ vs. $^{38}Ar_{Cl}/^{39}Ar_K$ for in vacuo crushing data of the quartz samples. $^{40}Ar^*$ yield strong correlation with $^{38}Ar_{Cl}$ in the initial crushing steps. Crushing steps were numbered to show the sequence of crushing. Only the steps that defining the age plateaux (pink points) and the $^{40}Ar^*/^{38}Ar_{Cl}$ line (green points) are shown.

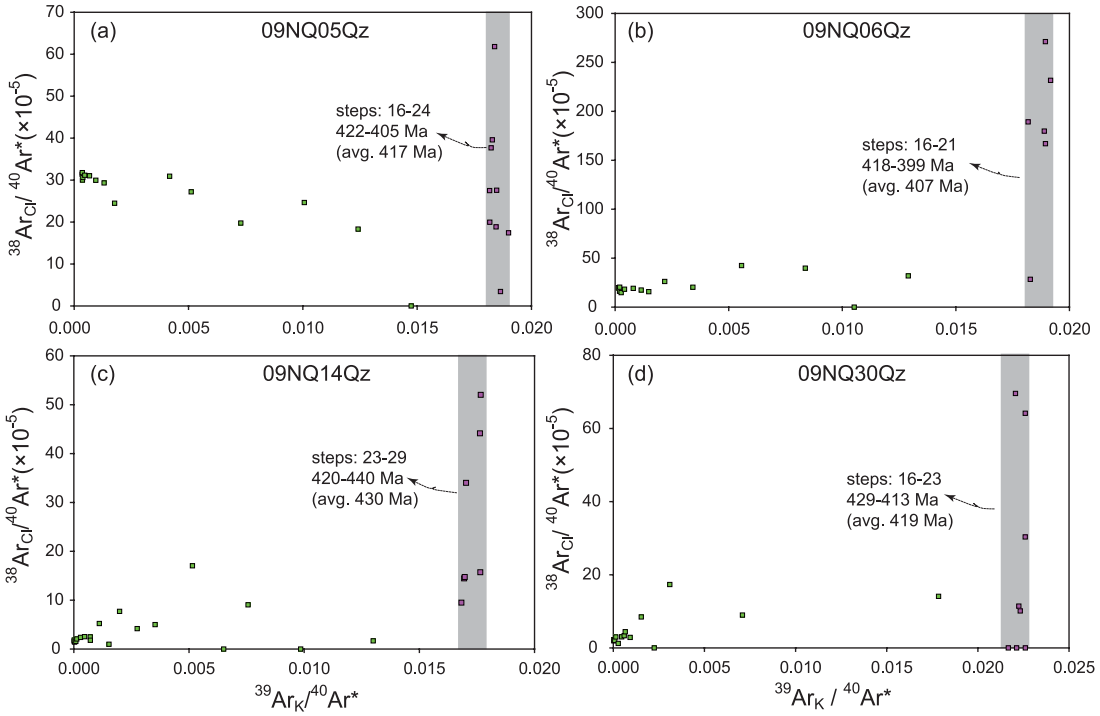

Fig. 8. Plots of $^{38}Ar_{Cl}/^{40}Ar^*$ vs. $^{39}Ar_K/^{40}Ar^*$ for individual crushing measurements on quartz samples.

first several steps are too scattered to form correlation lines (Fig. 6, green points). As expected, the data points that contribute to the age plateaus define correlation lines with slopes corresponding to Silurian ages of 412, 418, 440 and 420 Ma, for samples 09NQ05Qz, 09NQ06Qz, 09NQ14Qz and 09NQ30Qz, respectively (Fig. 6, pink points). These ages are in good agreement with the corresponding plateau ages.

$^{40}Ar^*/^{39}Ar_K$ vs. $^{38}Ar_{Cl}/^{39}Ar_K$

On the plots of $^{40}Ar^*/^{39}Ar_K$ vs. $^{38}Ar_{Cl}/^{39}Ar_K$ as shown in Fig. 7, the data points of the first steps show good linear correlations with $^{40}Ar^*/^{39}Ar_K$ intercepts of 35.8–51.1, corresponding to Devonian–Carboniferous ages of 392–341 Ma (Fig. 7, green points). By contrast, the data points defining the age plateaus with lower $^{38}Ar_{Cl}$ values and without any apparent correlation between $^{40}Ar^*/^{39}Ar_K$ and $^{38}Ar_{Cl}/^{39}Ar_K$ (Fig. 7, pink points), indicate a distinctly different domain for the gas of plateau age steps. The data points show relatively constant $^{40}Ar^*/^{39}Ar_K$ ratios of 59–44, corresponding to individual ages from 440 to 399 Ma and average ages from 430 to 407 Ma, respectively.

$^{38}Ar_{Cl}/^{40}Ar^*$ vs. $^{39}Ar_K/^{40}Ar^*$

As noted previously, unlike the $^{40}Ar^*$ component, the $^{39}Ar_K$ does not yield any apparent correlation with the $^{38}Ar_{Cl}$ (Fig. 8). As shown in the plots of $^{38}Ar_{Cl}/^{40}Ar^*$ vs. $^{39}Ar_K/^{40}Ar^*$, the data points that have been selected as defining the age plateaus and isochrons are showing relatively constant values of $^{38}Ar_{Cl}/^{40}Ar^*$ but wide range of $^{39}Ar_K/^{40}Ar^*$ ratios (Fig. 8, green points). In contrast, the late crushing steps show concordant $^{39}Ar_K/^{40}Ar^*$ ratios but variable $^{38}Ar_{Cl}/^{40}Ar^*$ ratios (Fig. 8, pink points). The $^{39}Ar_K/^{40}Ar^*$ ratios are ranging from 0.017 to 0.023 with average ages from 430 to 407 Ma, representing the ages of PFIs.

Discussion

Veining stage

Quartz samples in this study are almost pure quartz veins (95%) and crosscut eclogite blocks in random directions. An exception is the sample 09NQ14Qz, whose quartz contents are clearly lower (85%) and that occurs as sheet on the surface of an eclogite block (Fig. 2a). The mineral paragenesis indicates retrograde assemblages including amphibole and white mica. Therefore, from the petrological relationship between quartz vein and host rocks, as well as the mineral assemblage characteristics, all quartz veins analysed in this study belong to the group of late retrograde veins, that formed near the end of retrograde metamorphism (Li *et al.*, 2001a; Zheng, 2004). In contrast, quartz in eclogite or granulite lithologies that were formed during UHP metamorphic stage commonly contains gaseous fluids (i.e., N_2–CH_4, etc.). These are interpreted as syn-metamorphic fluids that could be the

remnants of pre-metamorphic pore fluids or prograde pore fluids (Andersen *et al*., 1993; Fu *et al*., 2003). In this study, no such fluids were detected in any of the Yuka quartz veins, which was taken as indirect evidence that the Yuka veins have not experienced UHP metamorphism but formed during exhumation.

Gas release pattern and argon reservoirs

An experimental crushing test has been accomplished by Bai *et al*. (2013), that stages that after more than 10,000 pestle drops, the crushed quartz residue ranges in grain size from 4–1 μm (82%), and the powder contains fragments as small as 50 nm. The primary fluid inclusions in Yuka quartz are mostly in the range 15–5 μm in size (Fig. 3). This indicates that the fluid inclusions in the size range that can be observed by optical microscope have effectively been extracted using the crushing method.

Anomalously old apparent ages are obtained from the early crushing steps, even older than the Earth's age, indicating that significant amounts of excee argon were incorporated in the fluid inclusions. Following the reasoning of Qiu and co-workers (Qiu and Wijbrans, 2006, 2008; Qiu and Jiang, 2007; Jiang *et al*., 2012; Bai *et al*., 2013), the SFIs can be easily liberated during the early crushing steps, due to their relatively large volume and distribution characteristics along crack. In contrast, the PFIs are isolated and randomly distributed in host crystals, only can be extracted with more impacts. Thus, we suggest that the extremely old initial apparent ages are derived from the largest, most easily crushed SFIs and that these were most likely incorporated in the quartz by a crack-seal mechanism during greenschist-facies retrogression, or later. As illustrated on Fig. 7, this component shows significant correlation between $^{40}Ar^*$ ($^{40}Ar_R + {}^{40}Ar_E$) and $^{38}Ar_{Cl}$. Because the entrapment of Cl in aqueous fluids generally leads to the correlation between neutron-induced $^{38}Ar_{Cl}$ and naturally occurring argon dissolved in the fluids, the correlation between $^{40}Ar^*$ and $^{38}Ar_{Cl}$ has been regarded as an effective indicator to monitor the degassing of fluid inclusions (Turner, 1988; Turner and Bannon, 1992; Harrison *et al*., 1993). Thus, the strong correlation between $^{40}Ar^*$ and $^{38}Ar_{Cl}$ not only confirms a fluid-related origin for the measured ages obtained in the stepwise crushing experiments but also indicates the excess ^{40}Ar ($^{40}Ar_E$) and Cl in the SFIs from the same source. The apparent ages that decrease gradually in the subsequent steps probably reflect mixtures between SFIs with excess ^{40}Ar and PFIs. In the final stages of the experiments, gas components are predominately derived from smaller PFIs. Mixtures of radiogenic argon from the PFIs and atmospheric argon from the crusher form a well-defined isochron and flat age plateau over the last several steps (see Fig. 4).

Origin of quartz vein hosted fluids

The Ar-isotopic compositions of fluid inclusions can be used to constrain the origin of fluids (Kelley *et al*., 1986; Turner and Bannon, 1992; Villa, 2001; Jiang *et al*., 2012). In this study, the gases that were released in the early and late crushing steps have quite different argon composition. Early liberated gases are rich in $^{40}Ar_E$ and $^{38}Ar_{Cl}$ whereas the late ones are poor in $^{40}Ar_E$ and $^{38}Ar_{Cl}$ but rich in $^{37}Ar_{Ca}$ and $^{39}Ar_K$ (see Table 2). We interpret the gases in the early steps were derived from SFIs and those in the late steps from PFIs. The PFIs show higher $^{37}Ar_{Ca}$ and $^{39}Ar_K$ but lower $^{38}Ar_{Cl}$, which suggests that lower chlorine and higher calcium and potassium contents are dissolved in the PFI fluid when compared with that dissolved in the SFI fluid. This fact may suggest that the PFIs reservoir was relatively poor in chlorine. However, microthermometric measurements show that the salinities of PFIs are higher than SFIs. Thus, the calcium and potassium in the PFIs are probably correlated with CO_3^{2-} and HCO_3^- rather than Cl^- dissolved in the vein-forming fluid (e.g., Jiang *et al*., 2012). This also can be used to explain the seemingly contradictory phenomenon that the higher salinity PFIs have lower $^{38}Ar_{Cl}$ whereas the lower salinity SFIs have higher $^{38}Ar_{Cl}$ signals.

There are several possible origins of the PFIs (type-a and type-b). Previous studies have argued that partial melting of both UHP rocks (eclogite) and host rocks (gneiss) during the stage of exhumation can induce a significant high salinity fluid flow that results in the precipitation of the quartz vein as well (e.g., Zong *et al*., 2010; Chen *et al*., 2012). Geochemical analyses show that the felsic veins in the Xitieshan terrane, north Qaidam, are tonalitic with high Na/K ratios, high Sr contents paired with low Y and Yb contents, and LREE-enriched patterns, consistent with partial melting of omphacite in eclogite at elevated pressures (Chen *et al*., 2012). Further, zircon Lu–Hf isotope investigation shows that the initial $^{176}Hf/^{177}Hf$ ratios of zircon rims from the quartz vein are lower than in zircons from an eclogite lens, but overlap with the coeval zircon domains from the nearby granite dikes produced by partial melting of orthogneiss. This suggests that the fluid flow responsible for quartz vein formation could be derived from the host gneiss during exhumation (Zong *et al*., 2010). Thereby, high salinity hydrothermal fluids produced during the partial melt of eclogite and host gneiss are the main origin of type-a fluids and one possible origin of type-b fluids, which were trapped during the amphibolite/greenschist-facies retrogression at the onset of quartz veining.

Aqueous fluid derived from the decomposition of hydrous minerals (e.g., lawsonite and zoisite) is also an important source of retrograde fluid (Li *et al*., 2001b; Zheng, 2004; Zheng *et al*., 2007). The release of water is not only triggered by the amphibolite/greenschist-facies

retrogression but also by quartz veining during exhumation of the continental crust. Therefore, it is possible that the intermediately saline PFIs (type-b) were derived from two mechanisms: partial melt of UHP rocks and dehydration of hydrous minerals. Moreover, the atmospheric initial $^{40}Ar/^{36}Ar$ ratios of the PFIs (see inverse isochron plot in Fig. 4) suggest that the meteoric water is an additional important source for the PFIs (e.g., Turner, 1988).

Dating by *in vacuo* crushing of vein quartz has demonstrated that the SFIs (type-c) contain a significant amount of excess ^{40}Ar ($^{40}Ar_E$). Deep metamorphic hydrothermal aqueous fluids commonly with high partial pressure of $^{40}Ar_E$ probably resulted from outgassing of crustal rocks during regional metamorphism (Turner, 1988; Turner and Bannon, 1992; Kelley, 2002). Thereby, the SFIs with excess ^{40}Ar were probably brought in by a post-hydrothermal fluid from the depth.

Implication of $^{40}Ar/^{39}Ar$ dating by in vacuo crushing

Trapping of fluid inclusions in quartz in HP/UHP rocks could occur during crystal first growth and during later stages by crack-seal mechanisms. Fluid inclusions in quartz that are trapped on sealed imperfection crystal surfaces during precipitation are consider as primary fluid inclusions, and the $^{40}Ar/^{39}Ar$ ages derived from these primary fluid inclusions are therefore regarded as approximating the time of quartz veining. Additionally, during exhumation, fluid flow that is resulting from protracted events in the crust such as diagenesis, retrogressed metamorphism and hydrothermal circulation following magma emplacement, could be trapped after quartz crystal growth when cracks develop. The $^{40}Ar/^{39}Ar$ ages derived from these fluid inclusions are then taken as the best estimate for the ages of hydrothermal activities during the lately exhumation stage of HP/UHP rocks.

Previous studies have shown that crushing has little effect on the gas trapped within the crystal lattice but predominately extract the gas that was trapped in fluid inclusions and along cracks and cavities in crystals (Dunlap and Kronenberg, 2001; Qiu and Wijbrans, 2006, 2008; Qiu and Jiang, 2007; Jiang *et al*., 2012; Bai *et al*., 2013). Therefore, the dating of fluid inclusions by the *in vacuo* crushing method in HP/UHP quartz minerals promises to be an effective means of dating the fluid as well as the age of veining if the two are related and nearly synchronous.

In the case of Yuka quartz samples, low salinity aqueous SFIs generally occur along cross-cutting healed fractures and are variable in size (see Fig. 3). As mentioned before, in the process gas-extraction by *in vacuo* crushing method, SFIs are easily crushed and liberated gases at the initial steps. Part of the bigger PFIs and pseudosecondary fluid inclusions which occur along the healed micro-cracks are probably also extracted during the same time. Consequently, due to mixing of gases originating from both SFIs and PFIs, SFIs on the isotope correlation diagram rarely show an isochron, although successful cases have been reported (Qiu and Jiang, 2007; Jiang *et al*., 2012). On the other hand, the $^{38}Ar_{Cl}$-based correlation diagram provides a potential approach for correlating the effect of excess ^{40}Ar within SFIs and further obtaining meaningful ages (Turner and Bannon, 1992; Jiang *et al*., 2012; Bai *et al*., 2013). As illustrated on the plots of $^{40}Ar^*/^{39}Ar_K^*$ vs. $^{38}Ar_{Cl}/^{39}Ar_K^*$ (see Fig. 7), the isochron ages of 392 Ma and ~344 Ma of the SFIs reveal episodes of post-collisional fluid flow activities during Middle Devonian and Early Carboniferous, respectively.

As crushing continues, the SFIs and excess ^{40}Ar were gradually exhausted whereas primary and pseudosecondary inclusions (type-b) dominate the gas contribution and yield concordant late Silurian plateau ages of 429–411 Ma for this stage (see age spectra in Fig. 4). The inclusions of type-b were trapped during the crystallization or recrystallization of quartz within the HP veins, and the gases liberated from these inclusions in the final stages of the experiments yielded geologically interpretable age results. Therefore, the plateau ages of 429–411 Ma can be taken as a good estimate for the time of quartz vein formation. That is, the $^{40}Ar/^{39}Ar$ dating by *in vacuo* crushing of HP quartz veins document a protracted Silurian fluid flow during the exhumation of HP/UHP rocks.

Similar ages of about 428 Ma were also obtained from the Xitieshan felsic vein via zircon U–Pb dating (Chen *et al*., 2012), indicating there is a synchronous fluid activity during the exhumation of UHP rocks in different parts of the North Qaidam UHP terrane. There are two cryptic tectono-thermal events during the late Silurian, which may have generated the post-collisional vein-forming fluid activity: (1) magmatic activity that was identified by zircon U–Pb dating of *ca*. 428 Ma in the north Qaidam orogen (Meng *et al*., 2005; Meng and Zhang, 2008); (2) regional ductile strike-slip shearing in the North Qaidam orogen that occurred between 426–401 Ma constrained by $^{40}Ar/^{39}Ar$ dating of foliated white mica (Qi, 2003; Menold, 2006; Xu *et al*., 2006).

Conclusions

Quartz veins are abundant in the Yuka eclogite–gneiss terrane, North Qaidam, where they provide vital information of the characteristics, origin and timing of fluid flow during the subduction/exhumation of the UHP metamorphic rocks.

1. Three categories of fluid inclusions have been recognized based on petrographic observation in Yuka quartz veins: hypersaline brine inclusions (type-a, primary), intermediate to high-salinity fluid inclusions (type-b, pri-

mary and pseudo-secondary) and low salinity aqueous fluid inclusions (type-c, secondary).

2. Due to the differences in distribution and size between SFIs and PFIs, when they are crushed, the gases are liberated in the early and later steps during crushing, respectively, and thus PFIs and SFIs can potentially be separated by stepwise crushing.

3. Type-a and type-b inclusions originate from mixed sources: dehydration of hydrous minerals, partial melt of eclogite and host rock, and meteoric water transported by fault/shear zones. Type-c fluid inclusions may have derive from deep metamorphic hydrothermal aqueous fluids.

4. There is an obvious correlation between excess ^{40}Ar and Cl in the secondary fluid inclusions. On the isotope correlation diagram of $^{40}Ar^*/^{39}Ar_K$ vs. $^{38}Ar_{Cl}/^{39}Ar_K$, the early data points form well-defined isochrons with two group intercept ages of 392 Ma and ~344 Ma.

5. The data points from the later of crushing *in vacuo* $^{40}Ar/^{39}Ar$ dating yield plateau ages of 429–411 Ma, indicating a protracted fluid flow during the exhumation of the Yuka HP/UHP rocks in the Silurian. A Silurian magmatic pulse in the area or regional ductile shearing may have caused this post-collisional fluid flow.

Acknowledgments—We appreciate the detailed and critical review by Dr. Masafumi Sudo, Dr. Tomoaki Morishita and an anonymous reviewer. We are also grateful to Dr. Takuya Matsumoto for his comments and editorial handling of the manuscript. The authors also would like to thank Mr. R. Van Elsas, Mrs. W. Koot, Mr. O. Postma, Mr. A. Bikker, and Mr. W. van der Plas for their kind help in mineral separation, thin section preparation, and technical support for the $^{40}Ar/^{39}Ar$ analyses. Financial support is from the Natural Science Foundation of China (41121002), the Chinese Academy Sciences - Royal Netherlands Academy of Arts and Sciences (CAS-KNAW) Joint PhD Training Programme (08PhD-08), and the Chinese Academy of Sciences (GIGCAS-135-Y234151001).

REFERENCES

Andersen, T., Austrheim, H., Burke, E. A. J. and Elvevold, S. (1993) N_2 and CO_2 in deep crustal fluids: evidence from the Caledonides of Norway. *Chem. Geol*. **108**, 113–132.

Bai, X. J., Wang, M., Jiang, Y. D. and Qiu, H. N. (2013) Direct dating of tin-tungsten mineralization of the Piaotang Tungsten deposit, South China, by $^{40}Ar/^{39}Ar$ progressive crushing. *Geochim. Cosmochim. Acta* **114**, 1–12.

Becker, H., Jochum, K. P. and Carlson, R. W. (1999) Constraints from high-pressure veins in eclogites on the composition of hydrous fluids in subduction zones. *Chem. Geol*. **160**, 291–308.

Birtel, S. and Stokhert, B. (2008) Quartz veins record earthquake-related brittle failure and short term ductile flow in the deep crust. *Tectonophysics* **457**, 53–63.

Chen, D. L., Sun, Y., Liu, L., Zhang, A. D., Luo, J. H. and Wang, Y. (2005) Metamorphic evolution of the Yuka eclogite in the North Qaidam, NW China:evidences from the compositional zonation of garnet and reaction texture in the rock. *Acta Petrol. Sin*. **21**, 1039–1048 (in Chinese with English abstract).

Chen, D. L., Sun, Y., Liu, L., Zhang, A. D. and Lin, C. L. (2007) *In situ* LA-ICP-MS zircon U–Pb age of ultrahigh-pressure eclogites in the Yukahe area, northern Qaidam Basin. *Sci. China, Ser. D Earth Sci*. **50**, 322–330.

Chen, D. L., Liu, L., Sun, Y. and Liou, J. G. (2009) Geochemistry and zircon U–Pb dating and its implications of the Yukahe HP/UHP terrane, the North Qaidam, NW China. *J. Asian Earth Sci*. **35**, 259–272.

Chen, D. L., Liu, L., Sun, Y., Sun, W. D., Zhu, X. H., Liu, X. M. and Guo, C. L. (2012) Felsic veins within UHP eclogite at xitieshan in North Qaidam, NW China: Partial melting during exhumation. *Lithos* **136–139**, 187–200.

Clay, P. L., Baxter, E. F., Cherniak, D. J., Kelley, S. P., Thomas, J. B. and Watson, E. B. (2010) Two diffusion pathways in quartz: A combined UV-laser and RBS study. *Geochim. Cosmochim. Acta* **74**, 5906–5925.

Dunlap, W. J. and Kronenberg, A. (2001) Argon loss during deformation of micas: constraints from laboratory deformation experiments. *Contrib. Mineral. Petrol*. **141**, 174–185.

Franz, L., Romer, R. L., Klemd, R., Schmid, R., Oberhänsli, R., Wagner, T. and Dong, S. W. (2001) Eclogite-facies quartz veins within metabasites of the Dabie Shan (eastern China): pressure-temperature-time-deformation path, composition of the fluid phase and fluid flow during exhumation of high-pressure rocks. *Contrib. Mineral. Petrol*. **141**, 322–346.

Fu, B., Touret, J. L. R., Zheng, Y. F. and Jahn, B. M. (2003) Fluid inclusions in granulites, granulitized eclogites and garnet clinopyroxenites from the Dabie–Sulu terranes, eastern China. *Lithos* **70**, 293–319.

Gao, T. S., Wang, S. S., Gong, B., Wu, Y. B. and Zheng, Y. F. (2006) Postcollisional flow of aqueous fluid within ultrahigh-pressure eclogite in the Dabie orogen. *J. Geochem. Explor*. **89**, 115–118.

Hall, D. L., Sterner, S. M. and Bodnar, R. J. (1988) Freezing-point depression of NaCl–KCl–H_2O solutions. *Econ. Geol*. **83**, 197–202.

Harrison, M., Matthew, H. and Oscar, L. (1993) *In vacuo* crushing experiments and K-feldspar thermochronometry. *Earth Planet. Sci. Lett*. **117**, 169–180.

Jiang, Y. D., Qiu, H. N. and Xu, Y. G. (2012) Hydrothermal fluids, argon isotopes and mineralization ages of the Fankou Pb–Zn deposit in south China: Insights from sphalerite $^{40}Ar/^{39}Ar$ progressive crushing. *Geochim. Cosmochim. Acta* **84**, 369–379.

John, T., Klemd, R., Gao, J. and Garbe Schoberg, C.-D. (2008) Trace-element mobilization in slabs due to non steady-state fluid-rock interaction: Constraints from an eclogite-facies transport vein in blueschist (Tianshan, China). *Lithos* **103**, 1–24.

Kelley, S. (2002) Excess argon in K–Ar and Ar–Ar geochronology. *Chem. Geol*. **188**, 1–22.

Kelley, S., Turner, G., Butterfield, A. W. and Shepherd, T. J. (1986) The source and significance of argon isotopes in fluid inclusions from areas of mineralization. *Earth Planet. Sci.*

Lett. **79**, 303–318.

Kendrick, M. A., Burgess, R., Pattrick, R. A. D. and Turner, G. (2001) Halogen and Ar–Ar age determinations of inclusions within quartz veins from porphyry copper deposits using complementary noble gas extraction techniques. *Chem. Geol*. **177**, 351–370.

Kendrick, M. A., Miller, J. M. and Phillips, D. (2006) Part II. Evaluation of ^{40}Ar–^{39}Ar quartz ages: Implications for fluid inclusion retentivity and determination of initial $^{40}Ar/^{36}Ar$ values in Proterozoic samples. *Geochim. Cosmochim. Acta* **70**, 2562–2576.

Koppers, A. (2002) ArArCALC-software for $^{40}Ar/^{39}Ar$ age calculations. *Comput. Geosci*. **28**, 605–619.

Li, S. G., Wang, S. S., Chen, Y. Z., Liu, D. L., Qiu, J., Zhou, H. X. and Zhang, Z. M. (1994) Excess argon in phengite from eclogite: Evidence from dating of eclogite minerals by Sm–Nd, Rb–Sr and $^{40}Ar/^{39}Ar$ methods. *Chem. Geol*. **112**, 343–350.

Li, Y. L., Zheng, Y. F. and Fu, B. (2001a) An oxygen isotope study of quartz veins within eclogites from the Dabie terrane. *Sci. China, Ser. D Earth Sci*. **44**, 621–634.

Li, Y. L., Zheng, Y. F., Fu, B., Zhou, J. B. and Wei, C. S. (2001b) Oxygen isotope composition of quartz-vein in ultrahigh-pressure eclogite from Dabieshan and implications for transport of high-pressure metamorphic fluid. *Phys. Chem. Earth Part A* **26**, 695–704.

Liu, X. C., Wu, Y. B., Gao, S., Liu, Q., Wang, H., Qin, Z. W., Li, Q. L., Li, X. H. and Gong, H. J. (2012) First record and timing of UHP metamorphism from zircon in the Xitieshan terrane: Implications for the evolution of the entire North Qaidam metamorphic belt. *Am. Mineral*. **97**, 1083–1093.

Mattinson, C. G., Menold, C. A., Zang, J. X. and Bird, D. K. (2007) High- and ultrahigh-pressure metamorphism in the North Qaidam and South Altyn Terranes, western China. *Int. Geol. Rev*. **49**, 969–995.

Meng, F. C. and Zhang, J. X. (2008) Contemporaneous of Early Paleozoic granite and high temperature metamorphism, North Qaidam Mountains, western China. *Acta Petrol. Sin*. **24**, 1585–1594 (in Chinese with English abstract).

Meng, F. C., Zhang, J. X. and Yang, J. S. (2005) Tectonothermal event of post-HP/UHP metamorphism in the Xitieshan area of the North Qaidam Mountians, western China: isotopic and geochemical evidence of granite and gneiss. *Acta Petrol. Sin*. **21**, 45–56 (in Chinese with English abstract).

Menold, C. A. (2006) Tectonic and metamorphic evolution of the North Qaidam ultrahigh-pressue metamorphic terrane, western China. Dr. Sci. Thesis, University of California., 261 pp.

Menold, C. A., Manning, C. E., Yin, A., Tropper, P., Chen, X. H. and Wang, X. F. (2009) Metamorphic evolution, mineral chemistry and thermobarometry of orthogneiss hosting ultrahigh-pressure eclogites in the North Qaidam metamorphic belt, Western China. *J. Asian Earth Sci*. **35**, 273–284.

Nelson, B. K. (1991) Sediment-derived fluids in subduction zones: Isotopic evidence from veins in blueschist and eclogite of the Franciscan Complex, California. *Geology* **19**, 1033–1036.

Nuhter, J.-A. and Stokhert, B. (2007) Vein quartz microfabrics indicating progressive evolution of fractures into cavities during postseismic creep in the middle crust. *J. Struct. Geol*. **29**, 1445–1462.

Qi, X. X. (2003) Large size ductile strike-slip shearing and the formation of Qilian Caledonian orogen. Dr. Sci. Thesis, Chinese Aeademy Geological Seience, 119 pp.

Qiu, H. N. and Jiang, Y. D. (2007) Sphalerite $^{40}Ar/^{39}Ar$ progressive crushing and stepwise heating techniques. *Earth Planet. Sci. Lett*. **256**, 224–232.

Qiu, H. N. and Wijbrans, J. R. (2006) Paleozoic ages and excess ^{40}Ar in garnets from the Bixiling eclogite in Dabieshan, China: New insights from $^{40}Ar/^{39}Ar$ dating by stepwise crushing. *Geochim. Cosmochim. Acta* **70**, 2354–2370.

Qiu, H. N. and Wijbrans, J. R. (2008) The Paleozoic metamorphic history of the Central Orogenic Belt of China from $^{40}Ar/^{39}Ar$ geochronology of eclogite garnet fluid inclusions. *Earth Planet. Sci. Lett*. **268**, 501–514.

Qiu, H. N., Zhu, B. Q. and Sun, D. Z. (2002) Age significence interpreted from dating of quartz samples from the Dongchuan Copper Deposits, Yunnan, SW China, by crushign and heating. *Geochem. J*. **36**, 475–491.

Roedder, E. (1984) *Fluid Inclusions (Reviews in Mineralogy 12)*. Mineralogical Society of America, Washington, D.C., 644 pp.

Rubatto, D. and Hermann, J. (2003) Zircon formation during fluid circulation in eclogites (Monviso, Western Alps): implications for Zr and Hf budget in subduction zones. *Geochim. Cosmochim. Acta* **67**, 2173–2187.

Rubatto, D., Gebauer, D. and Compagnoni, R. (1999) Dating of eclogite-facies zircons: the age of Alpine metamorphism in the Sesia–Lanzo Zone (Western Alps). *Earth Planet. Sci. Lett*. **167**, 141–158.

Schneider, B., Kuiper, K., Postma, O. and Wijbrans, J. (2009) $^{40}Ar/^{39}Ar$ geochronology using a quadrupole mass spectrometer. *Quat. Geochronol*. **4**, 508–516.

Selverstone, J., Franz, G., Thomas, S. and Getty, S. (1992) Fluid variability in 2 GPa eclogites as an indicator of fluid behavior during subduction. *Contrib. Mineral. Petrol*. **112**, 341–357.

Sheng, Y. M., Zheng, Y. F., Chen, R. X., Li, Q. L. and Dai, M. N. (2012) Fluid action on zircon growth and recrystallization during quartz veining within UHP eclogite: Insights from U–Pb ages, O–Hf isotopes and trace elements. *Lithos* **136**, 126–144.

Song, S. G., Zhang, L. F., Niu, Y. L., Su, L., Jian, P. and Liu, D. Y. (2005) Geochronology of diamond-bearing zircons from garnet peridotite in the North Qaidam UHPM belt, Northern Tibetan Plateau: A record of complex histories from oceanic lithosphere subduction to continental collision. *Earth Planet. Sci. Lett*. **234**, 99–118.

Turner, G. (1988) Hydrothermal fluids and argon isotopes in quartz veins and cherts. *Geochim. Cosmochim. Acta* **52**, 1443–1448.

Turner, G. and Bannon, M. P. (1992) Argon isotope geochemistry of inclusion fluids from granite-associated mineral veins in southwest and northeast England. *Geochim. Cosmochim. Acta* **56**, 227–243.

Villa, I. M. (2001) Radiogenic isotopes in fluid inclusions. *Lithos* **55**, 115–124.

Wang, D. H., Xu, J., Chen, Y. C., Li, H. Q. and Yu, J. J. (2003) Dating on the eclogite-hosted quartz crystal and its significance for tracing the exhumation history of the UHP belt in North Jiangsu. *Acta Geol. Sin*. **77**, 544–548 (in Chinese with English abstract).

Wang, S. S., Ge, N. J., Qiu, J. and Sang, H. Q. (2000) Isotopic ages of phengite from eclogite and quartz vein and their geological significance. *Prog. Nat. Sci*. **10**, 1024–1028 (in Chinese).

Wang, X. X., Hu, N. G., Castro, A., Wang, T. and Lu, X. X. (2013) Age, origin, and tectonic implications of Palaeozoic rapakivi granites in the North Qaidam orogen, Northwest China. *Int. Geol. Rev*. **55**, 1–22.

Wijbrans, J. R., Pringle, M. S., Koppers, A. A. P. and Scheveers, R. (1995) Argon geochronology of small samples using the Vulkaan argon laserprobe. *Proceedings Kon. Ned. Akaed. v. Wetensch* **98**, 185–218.

Wu, Y. B., Gao, S., Zhang, H. F., Yang, S. H., Liu, X. C., Jiao, W. F., Liu, Y. S., Yuan, H. L., Gong, H. J. and He, M. C. (2009) U–Pb age, trace-element, and Hf-isotope compositions of zircon in a quartz vein from eclogite in the western Dabie Mountains: Constraints on fluid flow during early exhumation of ultrahigh-pressure rocks. *Am. Mineral*. **94**, 303–312.

Xiao, Y. L., Hoefs, J., Van den Kerkhof, A. M., Simon, K., Fiebig, J. and Zheng, Y. F. (2002) Fluid evolution during HP and UHP metamorphism in Dabie Shan, China: Constraints from mineral chemistry, fluid inclusions and stable isotopes. *J. Petrol*. **43**, 1505–1527.

Xu, Z. Q., Yang, J. S., Wu, C. L., Li, H. B., Zhang, J. X., Qi, X. X., Song, S. G. and Qiu, H. J. (2006) Timing and mechanism of formation and exhumation of the Northern Qaidam ultrahigh-pressure metamorphic belt. *J. Asian Earth Sci*. **28**, 160–173.

Yang, J. S., Xu, Z., Song, S. G., Zhang, J. X., Wu, C. L., Shi, R. D., Li, H. B. and Brunel, M. (2001) Discovery of coesite in the North Qaidam Early Palaeozoic ultrahigh pressure (UHP) metamorphic belt, NW China. *Comptes Rendus de l'Academie des Sciences—Series IIA—Earth and Planetary Science* **333**, 719–724.

Yang, J. S., Liu, F. L., Wu, C. L., Xu, Z. Q., Shi, R. D., Chen, S. Y., Etienne, D. and Joseph, L. W. (2005) Two ultrahigh-pressure metamorphic events recognized in the central orogenic belt of China: Evidence from the U–Pb dating of coesite-bearing zircons. *Int. Geol. Rev*. **47**, 327–343.

Yardley, B. W. D. and Bottrell, S. H. (1992) Silica mobility and fluid movement during metamorphism of the Connemara schists, Ireland. *J. Metamorph. Geol*. **10**, 453–464.

Yin, A., Manning, C. E., Lovera, O., Menold, C. A. and Chen, X. H. (2007) Early paleozoic tectonic and thermomechanical evolution of ultrahigh-pressure (UHP) metamorphic rocks in the northern Tibetan plateau, northwest China. *Int. Geol. Rev*. **49**, 681–716.

Zhang, G. B., Ellis, D. J., Christy, A. G., Zhang, L. F., Ling, N. and Song, S. G. (2009) UHP metamorphic evolution of coesite-bearing eclogite from the Yuka terrane, North Qaidam UHPM belt, NW China. *Eur. J. Mineral*. **21**, 1287–1300.

Zhang, J. X., Yang, J. S., Mattinson, C. G., Xu, Z. Q., Meng, F. C. and Shi, R. D. (2005) Two contrasting eclogite cooling histories, North Qaidam HP/UHP terrane, western China: Petrological and isotopic constraints. *Lithos* **84**, 51–76.

Zhang, Z. M., Shen, K., Sun, W. D., Liu, Y. S., Liou, J. G., Shi, C. and Wang, J. L. (2008) Fluids in deeply subducted continental crust: Petrology, mineral chemistry and fluid inclusion of UHP metamorphic veins from the Sulu orogen, eastern China. *Geochim. Cosmochim. Acta* **72**, 3200–3228.

Zheng, Y. F. (2004) Fluid activity during exhumation of deep-subducted continental plate. *Chin. Sci. Bull*. **49**, 985–998.

Zheng, Y. F., Fu, B., Gong, B. and Li, L. (2003) Stable isotope geochemistry of ultrahigh pressure metamorphic rocks from the Dabie–Sulu orogen in China: implications for geodynamics and fluid regime. *Earth-Sci. Rev*. **62**, 105–161.

Zheng, Y. F., Gao, T. S., Wu, Y. B., Gong, B. and Liu, X. M. (2007) Fluid flow during exhumation of deeply subducted continental crust: zircon U–Pb age and O-isotope studies of a quartz vein within ultrahigh-pressure eclogite. *J. Metamorph. Geol*. **25**, 267–283.

Zheng, Y. F., Gao, X. Y., Chen, R. X. and Gao, T. S. (2011) Zr-in-rutile thermometry of eclogite in the Dabie orogen: Constraints on rutile growth during continental subduction-zone metamorphism. *J. Asian Earth Sci*. **40**, 427–451.

Zong, K. Q., Liu, Y. S., Hu, Z. C., Kusky, T., Wang, D. B., Gao, C. G., Gao, S. and Wang, J. Q. (2010) Melting-induced fluid flow during exhumation of gneisses of the Sulu ultrahigh-pressure terrane. *Lithos* **120**, 490–510.